

LETTER • OPEN ACCESS

Mixed-phase regime cloud thinning could help restore sea ice

To cite this article: D Villanueva *et al* 2022 *Environ. Res. Lett.* **17** 114057

View the [article online](#) for updates and enhancements.

You may also like

- [Assessing terrestrial biogeochemical feedbacks in a strategically geoengineered climate](#)
Cheng-En Yang, Forrest M Hoffman, Daniel M Ricciuto et al.
- [Strategic incentives for climate geoengineering coalitions to exclude broad participation](#)
Katharine L Ricke, Juan B Moreno-Cruz and Ken Caldeira
- [‘Bog here, marshland there’: tensions in co-producing scientific knowledge on solar geoengineering in the Arctic](#)
Ilona Mettäinen, Holly Jean Buck, Douglas G MacMartin et al.

ENVIRONMENTAL RESEARCH
LETTERS

LETTER

Mixed-phase regime cloud thinning could help restore sea ice

OPEN ACCESS

RECEIVED
18 August 2022REVISED
1 November 2022ACCEPTED FOR PUBLICATION
9 November 2022PUBLISHED
16 November 2022

Original Content from
this work may be used
under the terms of the
[Creative Commons
Attribution 4.0 licence](#).

Any further distribution
of this work must
maintain attribution to
the author(s) and the title
of the work, journal
citation and DOI.

D Villanueva^{1,2,*} , A Possner³, D Neubauer² , B Gasparini⁴ , U Lohmann² and M Tesche¹ ¹ Institute for Meteorology, Leipzig University, Leipzig, Germany² Institute for Atmospheric and Climate Science, ETH Zürich, Zurich, Switzerland³ Institute for Atmospheric and Environmental Sciences, Goethe University, Frankfurt am Main, Germany⁴ Department of Meteorology and Geophysics, University of Vienna, Vienna, Austria

* Author to whom any correspondence should be addressed.

E-mail: diego.villanueva@env.ethz.de**Keywords:** cloud geoengineering, aerosol-cloud interactions, glaciogenic seedingSupplementary material for this article is available [online](#)

Abstract

Cloud geoengineering approaches aim to mitigate global warming by seeding aerosols into clouds to change their radiative properties and occurrence frequency. Ice-nucleating particles (INPs) can enhance droplet freezing in clouds, reducing their water content. Until now, the potential of these particles has been mainly studied for weather modification and cirrus cloud thinning. Here, using a cloud-resolving model and a climate model we show that INPs could decrease the heat-trapping effect of mixed-phase regime clouds over the polar oceans during winter, slowing down sea-ice melting and partially offsetting the ice-albedo feedback. We refer to this concept as mixed-phase regime cloud thinning (MCT). We estimate that MCT could offset about 25% of the expected increase in polar sea-surface temperature due to the doubling of CO₂. This is accompanied by an annual increase in sea-ice surface area of 8% around the Arctic, and 14% around Antarctica.

1. Introduction

The global mean temperature is increasing as a result of human activities. This leads to a decrease in sea-ice cover, the melting of permafrost, and a decrease in planetary albedo—all effects that further accelerate warming (Lenton *et al* 2008, Stroeve *et al* 2012, Turetsky *et al* 2019, Eayrs *et al* 2021). Geoengineering aims at mitigating global warming by either removing carbon dioxide from the atmosphere or by managing Earth's radiation budget. Managing the radiative balance of the planet could be done either directly—by placing reflecting aerosols or surfaces between the Sun and the Earth—or indirectly, by modifying clouds (Vaughan and Lenton 2011, Caldeira *et al* 2013, Latham *et al* 2013, Lawrence *et al* 2018). However, compared to a strategy seeking carbon neutrality, geoengineering has been received with skepticism, as it presents several disadvantages and risks (Robock *et al* 2008).

On average, high-level cirrus (ice) clouds have a warming effect by trapping heat that would otherwise escape to space, while low-level liquid clouds

have a cooling effect by reflecting solar radiation. Temperatures between 0 °C and −38 °C are referred to as the mixed-phase regime, where cloud water and ice can coexist. The corresponding mixed-phase regime clouds (MPRCs) can be pure-ice, pure-liquid, or mixed-phase clouds (MPCs), which contain both ice crystals and cloud droplets. In MPRCs, the heat trapping and solar reflection can compensate each other, so that the cloud radiative effect (CRE; positive for downward fluxes) can be positive or negative depending on the incoming solar radiation and the ice-to-liquid partition inside the cloud (Matus and L'Ecuyer 2017).

So far, two cloud-based geoengineering methods based on aerosol injections were proposed as options to slow down global warming. Aerosols can lead to droplet formation (>−38 °C; including supercooled droplets), droplet freezing (between 0 °C and −38 °C), or ice nucleation (<−38 °C). They can therefore affect the CRE (Twomey 1974) and cloud lifetime (Albrecht 1989). In marine cloud brightening, hygroscopic aerosols that act as cloud condensation nuclei are injected

into low-level warm clouds to increase the cloud droplet number concentration, leading to smaller droplets that reflect more solar radiation into space (Latham 1990). In cirrus cloud thinning, injecting ice-nucleating particles (INPs) in high-level cirrus clouds forces early ice nucleation at lower supersaturation and higher temperatures compared to unperturbed clouds. The resulting larger ice particles sediment faster and reduce the cloud's heat-trapping efficiency (Mitchell and Finnegan 2009). So far, the response of MPRCs to INP seeding was studied only indirectly for sedimenting ice due to cloud cirrus thinning (Gasparini *et al* 2017, Gruber *et al* 2019, Liu and Shi 2021, Tully *et al* 2022) and for the impact of shipping emissions (Christensen *et al* 2014, Possner *et al* 2017). Moreover, marine cloud brightening is not efficient during winter or over bright reflective surfaces. However, the Arctic ice cap is melting even more rapidly than projected (Senfleben *et al* 2020, Shu *et al* 2020). Thus, we are interested in exploring geoengineering concepts that can target the heat-trapping efficiency of clouds at high latitudes.

On one hand, multiple lines of evidence show that natural INPs such as mineral dust may enhance cloud glaciation in the troposphere (Villanueva *et al* 2020, 2021a, 2021b). On the other hand, artificial INPs such as silver iodide and dry ice have been used to trigger droplet freezing in MPRCs in a method called glaciogenic seeding (Schaefer 1946, Vonnegut and Chessin 1971, French *et al* 2018, Flossmann *et al* 2019). This process is employed for weather modification projects seeking to intensify precipitation or prevent hail formation (Dessens 1998, Qiu and Cressey 2008). However, the impact of glaciogenic seeding on precipitation is still a matter of open debate (Hobbs *et al* 1981, Kerr 1982, Miao and Geerts 2013, Tessendorf *et al* 2019).

After a few cloud droplets freeze, the resulting ice particles grow quickly due to the Wegener–Bergeron–Findeisen process (Heymsfield *et al* 2011, Findeisen *et al* 2015) and scatter less solar radiation compared to cloud droplets. These large ice particles fall faster than droplets, forming ice virgae or precipitation, which depletes the total water content (TWC) of the cloud. This cloud depletion results in a weaker cloud's heat-trapping, but also a weaker solar reflectivity. Thus, we are interested in identifying MPRCs with a net positive radiative effect dominated by heat-trapping, for which glaciogenic seeding could produce a net cooling effect. We refer to this geoengineering concept as mixed-phase regime cloud thinning (MCT).

2. Methods

2.1. Satellite data

For evaluating our climate model, we use a benchmark for the CRE of MPRCs obtained from

combining two A-Train products analogous to Villanueva *et al* (2021a) for the period 2007–2009. The cloud cover (CC) and cloud top temperature are based on the LiDAR-raDAR (DARDAR-MASK v2.0) product (Delanoë and Hogan 2010, Ceccaldi *et al* 2013). The dataset is collocated with the fifth release (R05) 2B-FLXHR-LIDAR algorithm (Matus and L'Ecuyer 2017) that uses retrieved cloud properties from CloudSat, CALIPSO, and MODIS to estimate the CRE. However, our analysis relates column CRE estimations directly to the cloud top temperature (in bins of 3 °C) with no differentiation of multi-layer or convective clouds. Both products are regridded to the same horizontal resolution as ECHAM-HAM ($1.875^\circ \times 1.875^\circ$) between 82.5° N/S.

2.2. Cloud-resolving simulations

As a first evaluation of the MCT concept, we carried out glaciogenic seeding experiments in cloud-resolving simulations of an Arctic stratocumulus deck during a cold air outbreak. We performed these large eddy simulations (group 'LES') with the idealized ICOSahedral Nonhydrostatic (ICON) model (Zängl *et al* 2014, Dipankar *et al* 2015) configured to reproduce observations during the Mixed-Phase Arctic Cloud Experiment (Verlinde *et al* 2007, Possner *et al* 2017). Except for the reference simulation, a fraction of the cloud droplets between 0.01% and 1% is forced to freeze per hour.

2.3. Climate simulations

To simulate the potential climate effect of MCT, we use the ECHAM-HAM climate model (Lohmann 2002, Neubauer *et al* 2019, Tegen *et al* 2019). The model includes Predicted Particle Property (P3) microphysics and a satellite simulator for cloud-phase observations (Bodas-Salcedo *et al* 2011, Morrison and Milbrandt 2015, Dietlicher *et al* 2018). ECHAM-HAM uses the PSrad radiation scheme (Pincus and Stevens 2013) and the RRTMG (Rapid Radiative Transfer Model for Global climate models) considering 16 shortwave bands (200 nm to $12\ \mu\text{m}$) and 14 longwave bands ($3\ \mu\text{m}$ to $1\ \text{mm}$). In the model, convective and stratiform precipitations are calculated separately. In ECHAM-HAM, our proxy for natural dust INPs reaches a 100% frozen fraction at about -27.5°C ('NS10K' simulation in Villanueva *et al* 2021b). At warmer temperatures, the fraction of dust-containing droplets that freeze decreases exponentially at a rate of four orders of magnitude per 10°C (Niemand *et al* 2012).

In this study, for temperatures warmer than -38°C , only immersion freezing is considered, as contact freezing (neglected in this study) is believed to be of secondary importance. We use an immersion freezing scheme derived from cloud chamber experiments (NS; e.g. Connolly *et al* 2009, Niemand *et al* 2012, Ickes *et al* 2017, Huang *et al* 2018). In this

Table 1. Summary of all simulations performed for this study, divided in four groups including N simulations each.

Model (GROUP)	Perturbation	Magnitude	N	Duration
ICON (LES)	Freezing rate [% h ⁻¹]	0, 10 ⁻² , 10 ⁻¹ , 1	4	1 d
ECHAM (FRZ)	Freezing rate [% h ⁻¹]	10 ⁻⁴ –10 ³	8	2 years
ECHAM (INP)	INP concentration [L ⁻¹]	10 ⁰ –10 ⁹	10	2 years
ECHAM (MLO)	Freezing rate [% h ⁻¹]	0 and 1	2	25 years

scheme, the fraction of frozen droplets FF increase with the INP surface area A_j and with the active surface site density n_s , which depends on temperature (T) and the INP characteristics N_A and N_B , with:

$$FF = 1 - e^{-A_j \cdot n_s(T)}, \quad (1)$$

$$n_s(T) = e^{-N_A \cdot (T - N_B)} [\text{m}^{-2}]. \quad (2)$$

Empirically, we set the temperature dependence ($N_A = 1^\circ\text{C}^{-1}$) and temperature offset ($N_B = +5^\circ\text{C}$) as proposed in Villanueva *et al* (2021b).

In our reference simulation (here called ‘REF’ simulation), ECHAM-HAM is configured to recreate the variability in cloud glaciation due to dust-aerosol, as observed from space (‘NS-Tuned’ simulation described in Villanueva *et al* 2021b). In the first group of sensitivity simulations (group ‘FRZ’), cloud droplets in the mixed-phase regime are forced to freeze with an additional rate between 10⁻⁴% and 10³% per hour. For rates higher than 10²% h⁻¹ all droplets (but no more) freeze within less than an hour (e.g. after only 6 min for 10³% per hour). The number of frozen droplets is updated at each model timestep (7.5 min). This perturbation neglects the temperature dependence of droplet freezing; however, it allows the assessment of all temperature levels at the same time, which would otherwise require several scenarios with varying INP activation temperature, and it is easier to replicate. The simulation with a freezing rate of 1% h⁻¹ is chosen as the optimal-seeding and called simply ‘SEED’. In a second group of sensitivity simulations (group ‘INP’), instead of enhancing droplet freezing homogeneously over all temperatures, the concentration of natural dust INP number is enhanced by 10⁰ l⁻¹ to 10⁹ l⁻¹ for the droplet freezing calculation, producing a droplet freezing rate that decreases exponentially with increasing temperature. Only the INP concentration in the immersion mode is perturbed, so that ice nucleation in the cirrus regime at temperatures colder than -38°C is unaffected.

In the ‘INP’ and ‘FRZ’ groups, the sensitivity simulations run for the period 2000–2001 and are nudged to observed meteorological conditions. In the third group of simulations (group ‘MLO’), to study the effect of MCT on sea-ice at equilibrium conditions, the simulations REF and SEED are coupled to a mixed-layer ocean model with interactive sea

surface temperature and run for 25 years (2001–2025) after a 25 year long spin-up time. A summary of the simulations used in this study can be found in table 1.

2.4. Analysis of cloud-resolving and climate simulations

For the cloud-resolving simulations ICON-LES, we analyzed how the reference cloudy region responds to glaciogenic seeding. Because the cloud deck filled the entire simulated region, we took the spatial average over the whole domain. This cloud deck remained stable after the first hour of simulation. Hence, we took the time average between hour 1 and hour 18 after the start of the simulation and the vertical average between 1150 m and 1900 m altitude, as this is where the reference cloud deck occurs. We excluded other vertical levels from the analysis, as no new cloud formation is observed outside the original cloudy layer.

The simulated CRE is calculated as the difference between the total and the clear-sky net radiative flux at the top of the atmosphere. The clear-sky component is derived during the simulations by recalculating the radiation transfer and ignoring the contribution of clouds. For the climate simulations with ECHAM-HAM, we use histograms of CRE and cloud top temperature at each model time step to study the radiative effect of MPRCs and how it may change due to MCT. These histograms are then averaged monthly for the analysis. In the case of multi-layer clouds, the cloud top temperature of the top-most cloud is considered—analogueous to the satellite data.

CRE_{all-sky}, which we refer to as CRE in this study, depends on the CC:

$$\text{CRE}_{\text{all-sky}} = \text{CRE}_{\text{cloudy}} \times \text{CC}. \quad (3)$$

Here, CRE_{cloudy} corresponds to the CRE in cloudy conditions. To understand the change in the radiative effect of MPRCs, we separate the component of CRE_{all-sky}:

$$\Delta \text{CRE}_{\text{all-sky}} \sim \text{CC} \times \Delta \text{CRE}_{\text{cloudy}} + \Delta \text{CC} \times \text{CRE}_{\text{cloudy}}. \quad (4)$$

The first term on the right-hand side of equation (4) represents the change dependent on CRE_{cloudy} and the second term the change dependent on CC (Chen *et al* 2014, Neubauer *et al* 2017).

For the 2 years nudged simulations, we assess the variability of the changes in CRE by using the regional standard deviation between horizontally adjacent gridboxes (Eight $1.875^\circ \times 1.875^\circ$ gridboxes for each 15° longitude). For the 25 years mixed-layer ocean simulations, we assess the uncertainty of the changes in precipitation, surface temperature, and sea-ice by calculating the signal-to-noise ratio (SNR) as:

$$\text{SNR} = \frac{\mu}{\sigma}, \quad (5)$$

where μ is the average change and σ is the standard deviation of the change between the 5 year running means (21 data points for the 25 year simulations). We discard changes with a SNR below one as not meaningful. A detailed extension of the methods above can be found in the supporting information.

3. Results

3.1. The heat-trapping effect of polar-marine liquid MPRCs

MPRCs are most frequent at high latitudes, polewards of 60° N/S (Zhang *et al* 2018). Figure 1 shows an evaluation of their radiative effect simulated with our climate model against satellite observations. The model is able to correctly represent the seasonal cycle of the CRE, mostly within one standard deviation of the observations. However, the warming effect of MPRCs is slightly underestimated during boreal winter and slightly overestimated during austral winter. For glaciogenic seeding, we consider months for which the average radiative effect of MPRCs is positive. This corresponds to the months November to February in the Northern Hemisphere and May to August in the Southern Hemisphere (referred from now on as winter for simplicity).

We focus on liquid-containing MPRCs, as only these are susceptible to droplet freezing. In our climate model, most liquid-containing MPRCs are pure-liquid, as only few clouds have a stable mixed-phase (Dietlicher *et al* 2019). For latitudes polewards of 45° N/S, liquid-containing MPRCs dominate over pure-ice clouds for temperatures warmer than -20°C in the Northern- and warmer than -33°C in the Southern Hemisphere, respectively. Figure 2 shows how the radiative effect of wintertime liquid-containing MPRCs varies between sea and land for different cloud top temperatures. Over land in the Northern Hemisphere, wintertime surface cooling reduces the difference between the temperature at the Earth's surface and the temperature at the top of MPRCs, which weakens their heat-trapping effect. Moreover, mineral dust particles acting as natural INPs emitted on land already increase the droplet freezing rate, reducing the impact of additional artificial INPs. As a result, winter MPRCs over land have

a very low warming effect at high latitudes ($60\text{--}90^\circ$ N; $0.7 \pm 0.4 \text{ W m}^{-2}$) and a cooling effect at mid-latitudes ($45\text{--}60^\circ$ N; $-2.2 \pm 0.9 \text{ W m}^{-2}$). Therefore, we consider only marine clouds as potential targets for glaciogenic seeding.

During winter, the column radiative effect of marine liquid-containing MPRCs at high latitudes ($60\text{--}90^\circ$ N/S; $4.5 \pm 0.7 \text{ W m}^{-2}$) is higher compared to mid-latitudes ($45\text{--}60^\circ$ N/S; $0.7 \pm 0.7 \text{ W m}^{-2}$). Moreover, between $45\text{--}60^\circ$ N/S, some winter liquid-containing MPRCs with tops warmer than -10°C have a net cooling effect. Thus, we target only marine clouds at latitudes polewards of 60° N/S.

3.2. Case study: glaciogenic seeding on an arctic MPRC

With our cloud-resolving model, we simulate a supercooled stratocumulus deck with an average cloud top temperature of -15°C and how it responds to artificial droplet freezing. Without perturbations, as the supercooled droplets freeze and the formed ice crystals grow, they fall down producing a total accumulated surface precipitation of 0.44 mm within 18 h . Table 2 shows how the simulated cloud deck develops for different artificial droplet freezing rates. For an artificial droplet freezing rate of $0.01\% \text{ h}^{-1}$, the TWC of the cloud deck is reduced by 21% , which weakens its solar radiative effect from -24 W m^{-2} to -22 W m^{-2} . A higher artificial freezing rate of $0.1\% \text{ h}^{-1}$ reduces the original cloud water by 88% and increases the accumulated precipitation by 57% . As a result, much of the cloud liquid is depleted, and a considerable mass fraction of the remaining cloud (41%) is composed of ice particles. In addition, the terrestrial radiative effect of the cloud decreases by 18 W m^{-2} , while its solar radiative effect weakens merely by 10 W m^{-2} . For a freezing rate of $1\% \text{ h}^{-1}$ almost all cloud water (i.e. 95%) is depleted. Even though the cloud still covers 22% of the simulated region, its terrestrial radiative effect decreases to only 3 W m^{-2} , resulting in a net cooling effect of 33 W m^{-2} compared to the reference without seeding.

3.3. Glaciogenic seeding on polar-marine MPRCs during winter

Figure 3(a) shows the change in the total CRE over oceans for different artificial freezing rates in MPRCs compared to the reference simulation without perturbations. This also includes the indirect response of warm and cirrus clouds (outside the range between -38°C and 0°C) to changes in the droplet freezing of MPRCs (e.g. through changes in humidity and atmospheric stability). For artificial freezing rates between $10^{-4}\% \text{ h}^{-1}$ and $1\% \text{ h}^{-1}$, the resulting cooling increases logarithmically. The cooling maximizes at $1\% \text{ h}^{-1}$ and decreases for rates higher than $100\% \text{ h}^{-1}$ (i.e. all droplets freeze within less than an

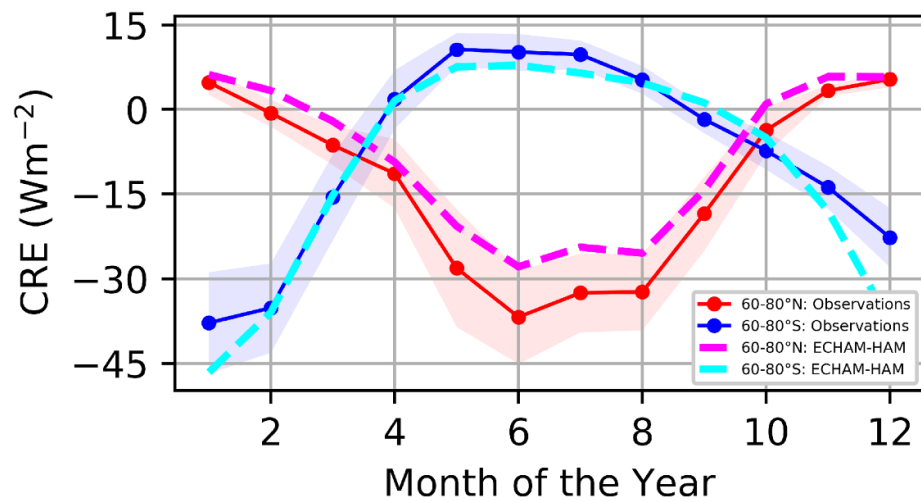


Figure 1. Simulated ('REF' simulation with ECHAM-HAM; 2000–2001) and observed (2B-FLXHR-LIDAR) cloud radiative effect (CRE) of MPRCs at high latitudes over the Northern Hemisphere and Southern Hemisphere. The shaded areas corresponds to the standard deviation between the daily averages of the 4 year observation period.

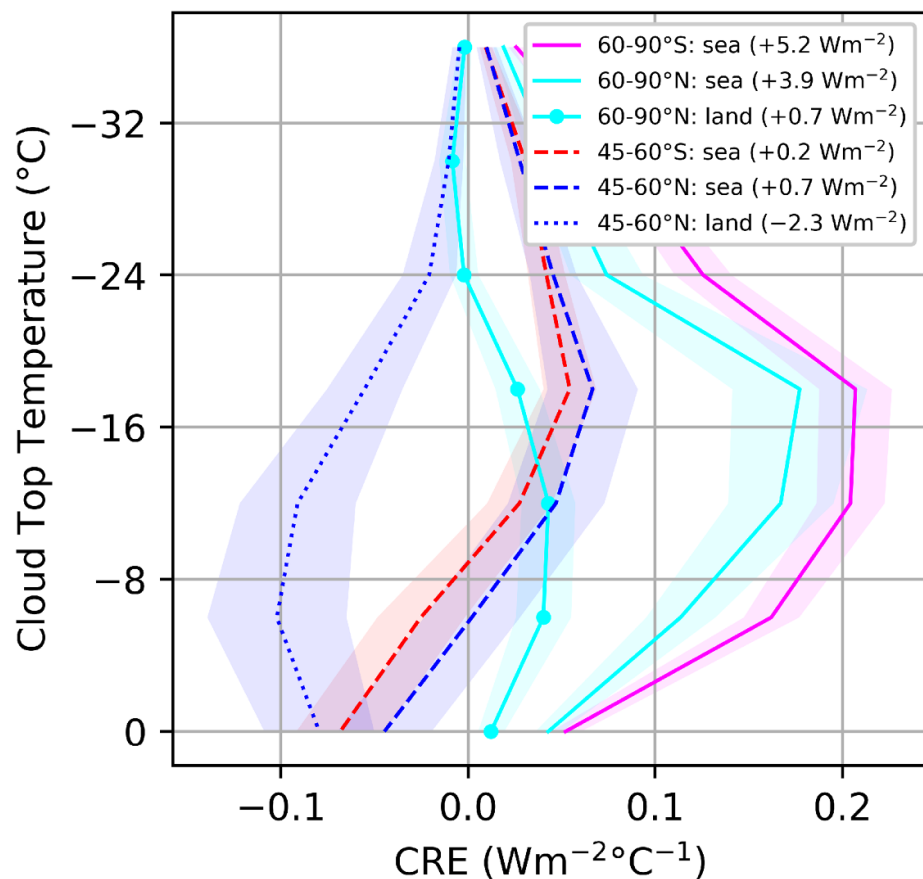


Figure 2. Simulated cloud radiative effect (CRE) of liquid-containing MPRCs during winter over the Northern Hemisphere and Southern Hemisphere for different latitude bands ('REF' simulation with ECHAM-HAM; 2000–2001). The radiative effect is normalized by the width of the intervals of cloud top temperature [°C]. The column-integrated cloud radiative effect given in the legend corresponds to the weighted sum over the entire range of cloud top temperatures. Pure-ice clouds are excluded, but pure-supercooled liquid clouds are included. The shaded area corresponds to the zonal standard deviation of neighboring gridboxes within 15° intervals.

hour) likely due to additional droplet freezing preventing the growth of ice crystals and their sedimentation. Therefore, we choose a freezing rate of $1\% \text{ h}^{-1}$ as our optimal-seeding (SEED) simulation.

For the Arctic Ocean, we consider the region between 60° N – 90° N (60° N – 75° N for figure 3) and between 30° W – 90° E . For the Southern Ocean, we consider the whole latitude band between 60° – 75° S .

Table 2. Results of cloud-resolving simulations (group LES) for an Arctic stratocumulus deck with an average cloud top at -15°C . In the simulations, an additional fraction of the cloud droplets between 0.01% and 1% is forced to freeze per hour. TWC: total water content; LW CRE: longwave (terrestrial) cloud radiative effect; CC: cloud cover; SW CRE: shortwave (solar) cloud radiative effect.

Freezing rate $\% \text{ h}^{-1}$	TWC g kg^{-1}	Precipitation accumulated mm	SW CRE W m^{-2}	LW CRE W m^{-2}	Supercooled fraction %	CC %
0 (ref)	0.170	0.44	−24	57	99	99
0.01	0.135	0.45	−22	57	87	99
0.1	0.038	0.69	−12	39	59	96
1	0.009	0.73	−3	3	35	22

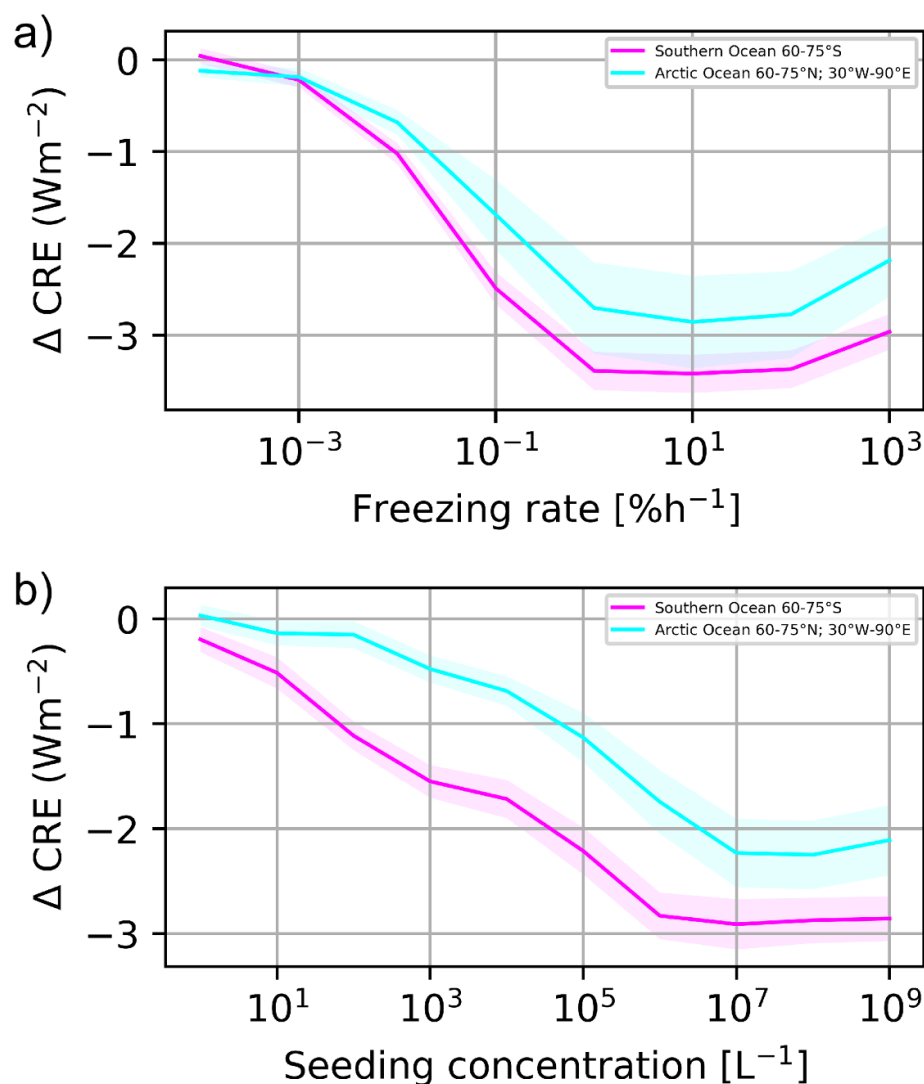


Figure 3. Change in the total cloud radiative effect (CRE) (also including warm and cirrus clouds) during winter over the Southern and Arctic Ocean between $60\text{--}75^{\circ}$ N/S for (a) an enhancement in the droplet freezing rate (group FRZ), and (b) constant seeding concentrations of natural dust INPs (group INP). The perturbation is limited to MPRCs and simulated with ECHAM-HAM (2000–2001). The shaded area corresponds to the zonal standard deviation of neighboring gridboxes within 15° intervals.

These regions capture most of the sea-ice-free area over ocean during winter. For the latitudes between $60\text{--}75^{\circ}$ N/S, the induced cooling over the Southern Ocean is stronger than over the Arctic Ocean. This is because the Arctic Ocean is affected by long-range transport of desert dust INPs (Shi *et al* 2022), which results in less frequent liquid-dominated clouds

susceptible to droplet freezing (Villanueva *et al* 2021a).

For seeding scenarios with a single INP type, the droplet freezing rate decreases exponentially with increasing temperature, resulting in freezing rates too high at low temperatures and too low at high temperatures compared to SEED. Figure 3(b) shows the

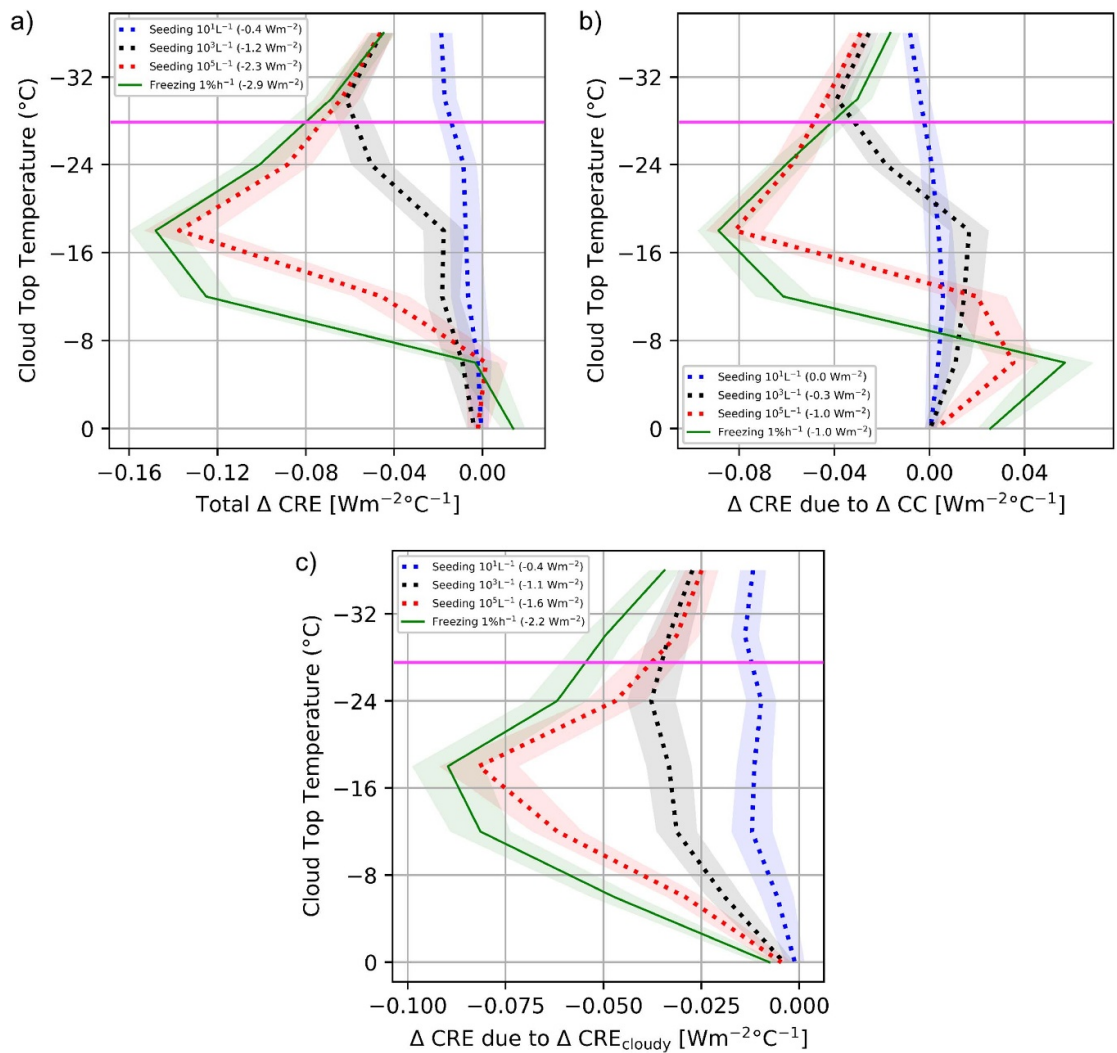


Figure 4. Change in the cloud radiative effect (CRE) for mixed-phase clouds between 60–75° S (Southern Ocean) simulated with ECHAM-HAM (2000–2001) during winter and normalized by the range of the temperature intervals. The profiles correspond to the simulation with artificial droplet freezing rate (1% h⁻¹; ‘SEED’), or with constant seeding concentrations of natural dust INPs (10¹ l⁻¹, 10³ l⁻¹, and 10⁵ l⁻¹). The change is separated into (a) total change, (b) changes in cloud cover (CC), and (c) changes in CRE_{cloudy}. The column-integrated change in cloud radiative effect ΔCRE shown in parentheses on the legend corresponds to the weighted sum over the entire cloud temperature range. The shaded area corresponds to the zonal standard deviation of neighboring gridboxes within 15° intervals. The horizontal pink line shows the temperature below which 100% of natural dust is active as INP (−27.5 °C).

change in the total CRE over oceans for different seeding concentrations of natural dust INP, including warm and cirrus clouds. The cooling increases logarithmically for increasing concentrations and maximizes at 10⁷ l⁻¹. Compared to the SEED simulation, concentrations of 10⁷ l⁻¹ lead to only 85% and 78% of the cooling over the Southern Ocean and Arctic Ocean, respectively. Over the Southern Ocean, the average dust concentrations vary around 10¹ l⁻¹ (Maloney *et al* 2022). In the Northern Hemisphere, dust concentrations vary from about 10³ l⁻¹ during non-dusty conditions over the Arctic Ocean (Kupiszewski *et al* 2013, Dagsson-Waldhauserova *et al* 2019) to 10⁵ l⁻¹ for dust-dominated conditions such as inside the Saharan Air Layer over the subtropical Atlantic (Renard *et al* 2018). Concentrations of

10⁷ l⁻¹ are unprecedented in the atmosphere and should therefore not be considered.

Figure 4(a) shows the change in the radiative effect of marine MPRCs between 60–75°S for the SEED simulation, and for simulations with enhanced concentrations of natural dust. Figures 4(b) and (c) show the change in CRE attributed to changes in CC and CRE_{cloudy}, respectively. For artificially enhanced concentrations of fine natural dust (10³ l⁻¹ and 10⁵ l⁻¹), the cooling effect over the Southern Ocean (60–75° S) is lower (43% and 80% of the effect in SEED, respectively; figure 4(a). This is caused by a weaker cooling effect due to MCT for clouds with cloud tops warmer than −30 °C and −18 °C for natural dust seeding of 10³ and 10⁵ l⁻¹, respectively, when compared to SEED. Over

the Arctic Ocean, the cooling effect is even lower compared to SEED (16% and 50%, respectively; not shown), because the few liquid-dominated clouds that persist occur at warmer temperatures, where natural dust INPs are less efficient. These clouds are nevertheless susceptible to droplet freezing in the SEED simulation, where the freezing rate is constant for all temperatures.

To better understand MCT, we analyze the contributions of CC and CRE_{cloudy} to the change in the CRE (equation (4)). On one hand, the increased sedimentation of ice particles decreases the fractional cover of MPRCs. However, as ice particles sediment below the cloud layer they sublimate and release water vapor, increasing the humidity and CC at lower levels. In contrast, we discard a strong seeder-feeder effect when ice particles reach a second cloud (feeder) below the original cloud (seeder), as this would likely enhance cloud depletion producing a lower CC at temperatures warmer than -10°C . For austral marine clouds, in the SEED simulation the change in the CRE due to changes in CC is positive for cloud tops warmer than -10°C (figure 4(b)), likely due to sublimating ice virgae. Thus, for increasing seeding concentrations of natural dust INPs—where droplet freezing decreases at warmer temperatures—the increase in the CRE due to a higher CC occurs at increasingly warmer temperatures (see seeding simulations with dust concentrations of 10^1 l^{-1} , 10^3 l^{-1} , and 10^5 l^{-1} in figure 4(b)).

On the other hand, the reduction in the cloud water content in MPRCs reduces their CRE_{cloudy} . The change in the CRE due to reductions in CRE_{cloudy} is proportional to the average radiative effect of MPRCs, with the strongest cooling at -18°C in the SEED simulation (figure 4(c)). For marine MPRCs between 60° – 75°S , the column-integrated change in the CRE due to the reduction in CRE_{cloudy} is about twice as strong compared to the radiative change associated to changes in CC.

In our simulations, the artificial seeding was only considered for droplet freezing calculations. However, concentrations of 10^5 l^{-1} would produce a considerable direct radiative effect through the absorption of terrestrial radiation by aerosols (Dufresne *et al* 2002). More efficient INPs—such as silver iodide—would activate at warmer temperatures and require at least four orders of magnitude lower number of seeded particles (Marcolli *et al* 2016). In addition, concentrations below 10^3 l^{-1} would produce a suboptimal cooling effect even if all seeded INP are active, as the droplet freezing rate will still be limited by the aerosol number concentration (see figure 4(a) for temperatures below -27.5°C). Thus, our results suggest that seeding concentrations of very efficient INPs such as silver iodide at 10^3 l^{-1} could both maximize the cooling effect of MCT and

minimize undesired aerosol effects. However, compared to dust INPs, even less is known about the effect of artificial aerosol such as silver iodide in the real atmosphere.

3.4. Cooling over the polar oceans, sea-ice enhancement, and impacts on the water cycle

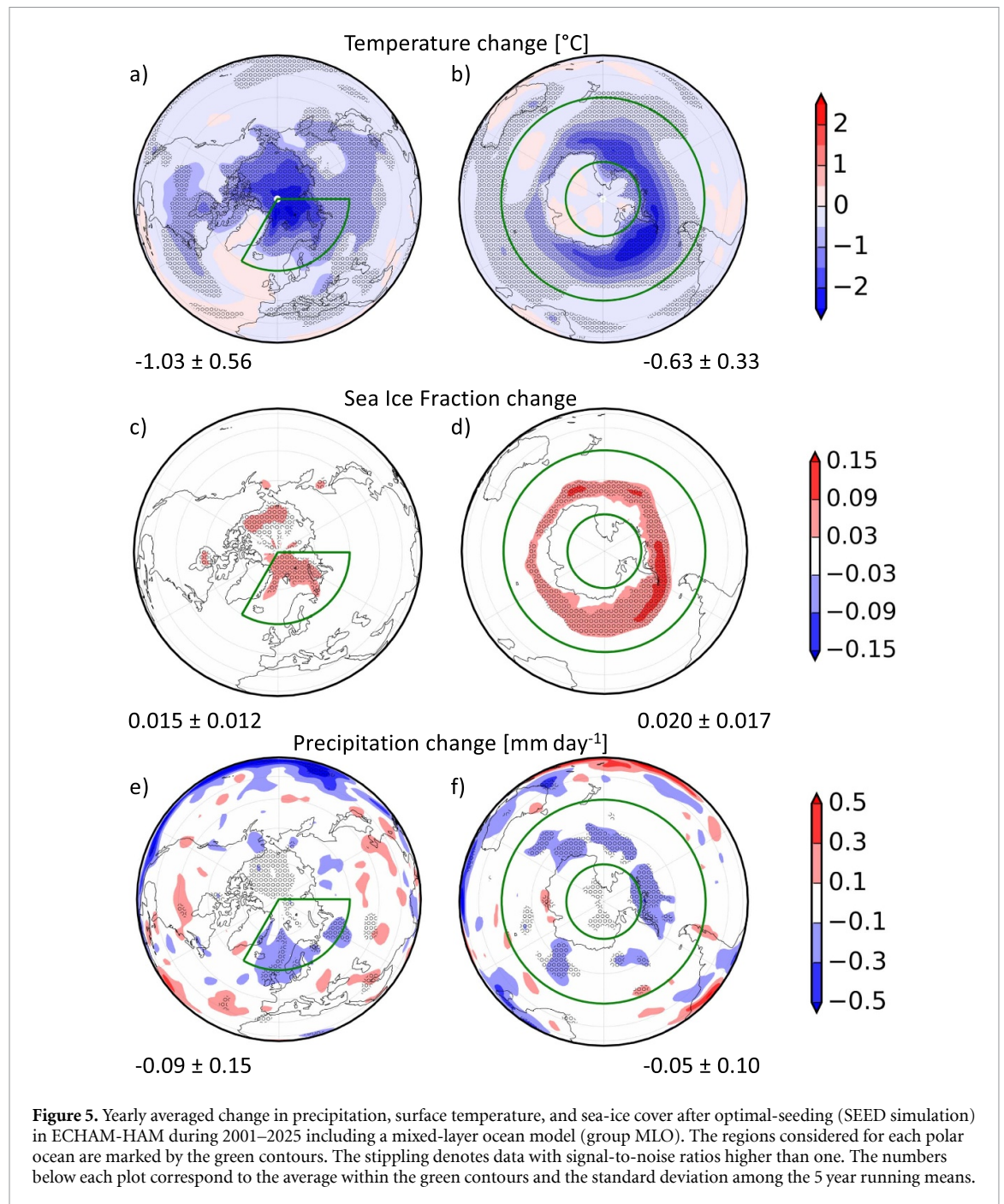
Figure 5 shows the main climatological changes due to MCT for the SEED simulation. The annual mean surface temperature decreases by $-1.03 \pm 0.57^{\circ}\text{C}$ over the Arctic Ocean (figure 5(a)) and by $-0.63 \pm 0.33^{\circ}\text{C}$ over the Southern Ocean (figure 5(b)). Thus, over these marine regions, the magnitude of the cooling could offset 25% of the expected warming produced by CO_2 doubling (Neubauer *et al* 2019).

MCT increases the winter sea-ice cover, especially around Antarctica. Over the studied Arctic Ocean region, the annual mean sea-ice surface area increases by 8%, increasing by 32% during boreal winter and decreasing by -39% during boreal summer (see figure 5(c)). This rebound effect is likely due to an increased poleward heat transport resulting from the cooling at the surface. In the Southern Ocean, the annual mean sea-ice surface area increases by 14%, increasing by 36% during austral winter and decreasing by -55% during austral summer (figure 5(d)). Because of the larger area covered by the Southern Ocean, the absolute increase in sea-ice surface area is four times as large compared to the increase in the entire Northern Hemisphere.

MCT changes the water balance in the atmosphere, especially regarding the cloud water path and convective precipitation. During austral winter, the cloud water path in the SEED simulation decreases by -13% and the CC decreases by -4% . In the SEED simulation, the total annual precipitation decreases by -3% (figure 5(e)). The convective component of the precipitation decreases by -14% and the stratiform component decreases by -2% (not shown). The decrease in convective precipitation is likely related to the increase in thermal stability as a result of the cooling near the Earth's surface. This is accompanied by a -20% decrease in the maximum convective updraft speed. Other than expected, in the SEED simulation, glaciogenic seeding does not enhance precipitation (figure 5(e)), likely because the artificially formed ice crystals are generally too small to reach the ground. Moreover, in a cooler climate the hydrological cycle slows down, reducing the average precipitation.

4. Discussion

We find that—with the right timing and dosage—MCT has the potential to cool the surface over the Arctic and Southern Oceans. This cooling aids the recovery and persistence of the polar sea-ice during winter.



By studying the number and altitude of cloud droplets that freeze due to MCT, we can estimate how many aerosols would have to be injected and at which height. In the SEED simulation, assuming fine INPs of 0.1 μm diameter, the total number of droplets artificially frozen globally suggest a required aerosol injected mass of 0.15 Tg per year. Over the Southern Ocean, droplets freeze artificially at an average temperature of -10°C at about 1.4 km above the surface. Over the Arctic Ocean, they freeze at an average temperature of -17°C at about 1.9 km altitude. These heights are easily within the reach of currently available unmanned aircrafts (Axisa and DeFelice 2016).

Next to stratospheric aerosol injection, marine cloud brightening, and cirrus cloud thinning,

MCT offers a new alternative climate intervention method. To compare MCT with these geoengineering concepts, we first assess its strengths and related opportunities followed by its weaknesses and associated threats.

4.1. Strengths and opportunities

Similar to cirrus thinning, MCT is efficient during polar winter, when stratospheric aerosols and cloud brightening are not. For cirrus thinning, too many INPs may cause an overseeding effect that increases the warming effect of cirrus clouds (Gasparini and Lohmann 2016), but for MCT we found no overseeding risk associated with too high droplet freezing rates. In terms of its applicability, MCT would require

a lower injection height compared to cirrus thinning and stratospheric injections. Additionally, the aerosol injected for MCT would have a lower lifetime compared to stratospheric aerosols, as INPs would be deposited through ice sedimentation, allowing a quicker emergency shut-down. While stratospheric injections and cloud brightening propose a perturbation much larger than the natural effect of stratospheric sulfate (Andersson *et al* 2015) and of marine aerosols (Christensen *et al* 2016), the perturbation in MCT is closer to the natural effect of natural dust (Shi and Liu 2019, Villanueva *et al* 2021b), which simplifies its extrapolation from our current climate state.

4.2. Weaknesses and threats

MPRCs are less understood compared to cirrus or warm clouds, so that their response to perturbations are associated with a lower confidence. Immersion freezing is believed to dominate over contact freezing and was therefore neglected in this study. However, contact freezing could increase the MPC cooling effect observed for the constant seeding simulations, especially for MPRCs with warm cloud tops. Compared to other concepts, MCT has a much smaller target area, limited to high-latitude marine regions during winter. In terms of seeding magnitude, cloud brightening and stratospheric injections are also more scalable than MCT (Zhao *et al* 2021). In terms of its risks, the impact of MCT on the hydrological cycle and precipitation remains to be assessed with more confidence, as well as its impact on the ecosystem. Still, the main weakness of MCT remains the rebound effect of sea-ice during summer. However, complementing MCT with sea-ice enhancement strategies could extend the lifetime of sea-ice into the summer (Field *et al* 2018), making the concept feasible.

5. Conclusions

If society does not achieve net-zero greenhouse gas emissions in time to avoid global warming beyond manageable levels, climate intervention concepts might be the last resort to alleviate part of the climate damage caused by increasing greenhouse gases. Until then, cutting emissions remains the preferred strategy due to its limited risks (Robock *et al* 2008). Moreover, MCT may help mitigate the temperature rise over the poles due to melting sea-ice, which cannot be solved by carbon neutrality alone. Thus, the main potential of MCT is that it could avoid further decrease in sea-ice during warmer winters.

Data availability statement


The results of the simulations with ICON-LES and ECHAM-HAM, together with the satellite product

used to evaluate ECHAM-HAM are available at <https://doi.org/10.5281/zenodo.6979663>.


Acknowledgments

The instant profiles for the DARDAR and (R05) 2B-FLXHR-LIDAR products can be found in the AERIS/ICARE. We thank the developers of DARDAR and (R05) 2B-FLXHR-LIDAR for providing access to the products. We thank the ICARE Data and Services Center for facilitating the download of the instant profiles of the products. We thank the HAMMOZ community for providing access to the ECHAM-HAM model and the DKRZ for providing computational resources. The ECHAM-HAMMOZ model is developed by a consortium composed of ETH Zurich, Max Planck Institute for Meteorology, Forschungszentrum Jülich, University of Oxford, the Finnish Meteorological Institute, and the Leibniz Institute for Tropospheric Research. Finally, we thank all the scientific community behind the individual satellite missions.

ORCID iDs

D Villanueva  <https://orcid.org/0000-0003-3673-5706>

D Neubauer  <https://orcid.org/0000-0002-9869-3946>

B Gasparini  <https://orcid.org/0000-0002-7177-0155>

U Lohmann  <https://orcid.org/0000-0001-8885-3785>

M Tesche  <https://orcid.org/0000-0003-0096-4785>

References

- Albrecht B A 1989 Aerosols cloud microphysics and fractional cloudiness *Science* **245** 1227–30
- Andersson S M, Martinsson B G, Vernier J-P, Friberg J, Brenninkmeijer C A M, Hermann M, van Velthoven P F J and Zahn A 2015 Significant radiative impact of volcanic aerosol in the lowermost stratosphere *Nat. Commun.* **6** 7692
- Axisa D and DeFelice T P 2016 Modern and prospective technologies for weather modification activities: a look at integrating unmanned aircraft systems *Atmos. Res.* **178–179** 114–24
- Bodas-Salcedo A *et al* 2011 COSP: satellite simulation software for model assessment *Bull. Am. Meteorol. Soc.* **92** 1023–43
- Caldeira K, Bala G and Cao L 2013 The science of geoengineering *Annu. Rev. Earth Planet. Sci.* **41** 231–56
- Ceccaldi M, Delanoë J, Hogan R J, Pounder N L, Protat A and Pelon J 2013 From CloudSat-CALIPSO to earthcare: evolution of the DARDAR cloud classification and its comparison to airborne radar-lidar observations *J. Geophys. Res.: Atmos.* **118** 7962–81
- Chen Y-C, Christensen M W, Stephens G L and Seinfeld J H 2014 Satellite-based estimate of global aerosol–cloud radiative forcing by marine warm clouds *Nat. Geosci.* **7** 643–6
- Christensen M W, Chen Y and Stephens G L 2016 Aerosol indirect effect dictated by liquid clouds *J. Geophys. Res.: Atmos.* **121** 14636–50

- Christensen M W, Suzuki K, Zambri B and Stephens G L 2014 Ship track observations of a reduced shortwave aerosol indirect effect in mixed-phase clouds *Geophys. Res. Lett.* **41** 6970–7
- Connolly P J, Möhler O, Field P R, Saathoff H, Burgess R, Choularton T and Gallagher M 2009 Studies of heterogeneous freezing by three different desert dust samples *Atmos. Chem. Phys.* **9** 2805–24
- Dagsson-Waldhauserova P, Renard J-B, Olafsson H, Vignelles D, Berthet G, Verdier N and Duverger V 2019 Vertical distribution of aerosols in dust storms during the arctic winter *Sci. Rep.* **9** 1
- Delanoë J and Hogan R J 2010 Combined Cloudsat-CALIPSO-MODIS retrievals of the properties of ice clouds *J. Geophys. Res.* **115** D00H29
- Dessens J 1998 A physical evaluation of a hail suppression project with silver iodide ground burners in Southwestern France *J. Appl. Meteorol.* **37** 1588–99
- Dietlicher R, Neubauer D and Lohmann U 2018 Prognostic parameterization of cloud ice with a single category in the aerosol-climate model ECHAM(v6.3.0)-HAM(v2.3) *Geosci. Model Dev.* **11** 1557–76
- Dietlicher R, Neubauer D and Lohmann U 2019 Elucidating ice formation pathways in the aerosol-climate model ECHAM6-HAM2 *Atmos. Chem. Phys.* **19** 9061–80
- Dipankar A, Stevens B, Heinze R, Moseley C, Zängl G, Giorgetta M and Brdar S 2015 Large eddy simulation using the general circulation model icon *J. Adv. Model. Earth Syst.* **7** 963–86
- Dufresne J-L, Gautier C, Ricchiazzi P and Fouquart Y 2002 Longwave scattering effects of mineral aerosols *J. Atmos. Sci.* **59** 1959–66
- Eayrs C, Li X, Raphael M N and Holland D M 2021 Rapid decline in antarctic sea ice in recent years hints at future change *Nat. Geosci.* **14** 460–4
- Field L et al 2018 Increasing arctic sea ice albedo using localized reversible geoengineering *Earth's Future* **6** 882–901
- Findeisen W, Volken E, Giesche A M and Brönnimann S 2015 Colloidal meteorological processes in the formation of precipitation *Meteorol. Z.* **24** 443–54
- Flossmann A I, Manton M, Abshaev A, Bruintjes R, Murakami M, Prabhakaran T and Yao Z 2019 Review of advances in precipitation enhancement research *Bull. Am. Meteorol. Soc.* **100** 1465–80
- French J R, Friedrich K, Tessoroff S A, Rauber R M, Geerts B, Rasmussen R M, Xue L, Kunkel M L and Blestrud D R 2018 Precipitation formation from orographic cloud seeding *Proc. Natl Acad. Sci.* **115** 1168–73
- Gasparini B and Lohmann U 2016 Why cirrus cloud seeding cannot substantially cool the planet *J. Geophys. Res.: Atmos.* **121** 4877–93
- Gasparini B, Münch S, Poncet L, Feldmann M and Lohmann U 2017 Is increasing ice crystal sedimentation velocity in geoengineering simulations a good proxy for cirrus cloud seeding? *Atmos. Chem. Phys.* **17** 4871–85
- Gruber S, Blahak U, Haenel F, Kottmeier C, Leisner T, Muskatel H, Storelvmo T and Vogel B 2019 A process study on thinning of arctic winter cirrus clouds with high-resolution icon-art simulations *J. Geophys. Res.: Atmos.* **124** 5860–88
- Heymsfield A J, Thompson G, Morrison H, Bansemir A, Rasmussen R M, Minnis P, Wang Z and Zhang D 2011 Formation and spread of aircraft-induced holes in clouds *Science* **333** 77–81
- Hobbs P V, Lyons J H, Locatelli J D, Biswas K R, Radke L F, Weiss R R and Rangno A L 1981 Radar detection of cloud-seeding effects *Science* **213** 1250–2
- Huang W T K, Ickes L, Tegen I, Rinaldi M, Ceburnis D and Lohmann U 2018 Global relevance of marine organic aerosol as ice nucleating particles *Atmos. Chem. Phys.* **18** 11423–45
- Ickes L, Welti A and Lohmann U 2017 Classical nucleation theory of immersion freezing: sensitivity of contact angle schemes to thermodynamic and kinetic parameters *Atmos. Chem. Phys.* **17** 1713–39
- Kerr R A 1982 Cloud seeding: one success in 35 years *Science* **217** 519–21
- Kupiszewski P et al 2013 Vertical profiling of aerosol particles and trace gases over the central arctic ocean during summer *Atmos. Chem. Phys.* **13** 12405–31
- Latham J 1990 Control of global warming? *Nature* **347** 339–40
- Latham J, Kleypas J, Hauser R, Parkes B and Gadian A 2013 Can marine cloud brightening reduce coral bleaching? *Atmos. Sci. Lett.* **14** 214–9
- Lawrence M G, Schäfer S, Muri H, Scott V, Oschlies A, Vaughan N E, Boucher O, Schmidt H, Haywood J and Scheffran J 2018 Evaluating climate geoengineering proposals in the context of the paris agreement temperature goals *Nat. Commun.* **9** 1
- Lenton T M, Held H, Kriegler E, Hall J W, Lucht W, Rahmstorf S and Schellnhuber H J 2008 Tipping elements in the Earth's climate system *Proc. Natl Acad. Sci.* **105** 1786–93
- Liu J and Shi X 2021 Estimating the potential cooling effect of cirrus thinning achieved via the seeding approach *Atmos. Chem. Phys.* **21** 10609–24
- Lohmann U 2002 A glaciation indirect aerosol effect caused by soot aerosols *Geophys. Res. Lett.* **29** 4
- Maloney C, Toon B, Bardeen C, Yu P, Froyd K, Kay J and Woods S 2022 The balance between heterogeneous and homogeneous nucleation of ice clouds using CAM5/CARMA *J. Geophys. Res.: Atmos.* **127** e2021JD035540
- Marcolli C, Nagare B, Welti A and Lohmann U 2016 Ice nucleation efficiency of agi: review and new insights *Atmos. Chem. Phys.* **16** 8915–37
- Matus A V and L'Ecuyer T S 2017 The role of cloud phase in Earth's radiation budget *J. Geophys. Res.: Atmos.* **122** 2559–78
- Miao Q and Geerts B 2013 Airborne measurements of the impact of ground-based glaciogenic cloud seeding on orographic precipitation *Adv. Atmos. Sci.* **30** 1025–38
- Mitchell D L and Finnegan W 2009 Modification of cirrus clouds to reduce global warming *Environ. Res. Lett.* **4** 045102
- Morrison H and Milbrandt J A 2015 Parameterization of cloud microphysics based on the prediction of bulk ice particle properties. part I: scheme description and idealized tests *J. Atmos. Sci.* **72** 287–311
- Neubauer D, Christensen M W, Poulsen C A and Lohmann U 2017 Unveiling aerosol–cloud interactions—part 2: minimising the effects of aerosol swelling and wet scavenging in ECHAM6-HAM2 for comparison to satellite data *Atmos. Chem. Phys.* **17** 13165–85
- Neubauer D, Ferrachat S, Siegenthaler-Le Drian C, Stier P, Partridge D G, Tegen I, Bey I, Stanelle T, Kokkola H and Lohmann U 2019 The global aerosol–climate model ECHAM6.3–HAM2.3—part 2: cloud evaluation, aerosol radiative forcing and climate sensitivity *Geosci. Model Dev.* **12** 3609–39
- Niemand M et al 2012 A particle-surface-area-based parameterization of immersion freezing on desert dust particles *J. Atmos. Sci.* **69** 3077–92
- Pincus R and Stevens B 2013 Paths to accuracy for radiation parameterizations in atmospheric models *J. Adv. Model. Earth Syst.* **5** 225–33
- Possner A, Ekman A M L and Lohmann U 2017 Cloud response and feedback processes in stratiform mixed-phase clouds perturbed by ship exhaust *Geophys. Res. Lett.* **44** 1964–72
- Qiu J and Cressey D 2008 Meteorology: taming the sky *Nature* **453** 970–4
- Renard J-B, Dulac F, Durand P, Bourgeois Q, Denjean C, Vignelles D, Couté B, Jeannot M, Verdier N and Mallet M 2018 In situ measurements of desert dust particles above the western Mediterranean Sea with the balloon-borne Light Optical Aerosol Counter/sizer (LOAC) during the

- ChArMEx campaign of summer 2013 *Atmos. Chem. Phys.* **18** 3677–99
- Robock A, Jerch K and Bunzl M 2008 20 reasons why geoengineering may be a bad idea *Bull. At. Sci.* **64** 14–59
- Schaefer V J 1946 The production of ice crystals in a cloud of supercooled water droplets *Science* **104** 457–9
- Senfleben D, Lauer A and Karpechko A 2020 Constraining uncertainties in CMIP5 projections of september arctic sea ice extent with observations *J. Clim.* **33** 1487–503
- Shi Y and Liu X 2019 Dust radiative effects on climate by glaciating mixed-phase clouds *Geophys. Res. Lett.* **46** 6128–37
- Shi Y, Liu X, Wu M, Zhao X, Ke Z and Brown H 2022 Relative importance of high-latitude local and long-range-transported dust for arctic ice-nucleating particles and impacts on arctic mixed-phase clouds *Atmos. Chem. Phys.* **22** 2909–35
- Shu Q, Wang Q, Song Z, Qiao F, Zhao J, Chu M and Li X 2020 Assessment of sea ice extent in CMIP6 with comparison to observations and CMIP5 *Geophys. Res. Lett.* **47** 9
- Stroeve J C, Kattsov V, Barrett A, Serreze M, Pavlova T, Holland M and Meier W N 2012 Trends in arctic sea ice extent from CMIP5, CMIP3 and observations *Geophys. Res. Lett.* **39** L16502
- Tegen I *et al* 2019 The global aerosol–climate model ECHAM6.3–HAM2.3—part 1: aerosol evaluation *Geosci. Model Dev.* **12** 1643–77
- Tessendorf S A *et al* 2019 A transformational approach to winter orographic weather modification research: the snowie project *Bull. Am. Meteorol. Soc.* **100** 71–92
- Tully C, Neubauer D, Omanovic N and Lohmann U 2022 Cirrus cloud thinning using a more physically-based ice microphysics scheme in the ECHAM-HAM GCM *Atmos. Chem. Phys. Discuss.* **22** 11455–84
- Turetsky M R *et al* 2019 Permafrost collapse is accelerating carbon release *Nature* **569** 32–34
- Twomey S 1974 Pollution and the planetary albedo *Atmos. Environ.* (1967) **8** 1251–6
- Vaughan N E and Lenton T M 2011 A review of climate geoengineering proposals *Clim. Change* **109** 745–90
- Verlinde J *et al* 2007 The mixed-phase arctic cloud experiment *Bull. Am. Meteorol. Soc.* **88** 205–22
- Villanueva D, Heinold B, Seifert P, Deneke H, Radenz M and Tegen I 2020 The day-to-day co-variability between mineral dust and cloud glaciation: a proxy for heterogeneous freezing *Atmos. Chem. Phys.* **20** 2177–99
- Villanueva D, Neubauer D, Gasparini B, Ickes L and Tegen I 2021b Constraining the impact of dust-driven droplet freezing on climate using cloud-top-phase observations *Geophys. Res. Lett.* **48** 11
- Villanueva D, Senf F and Tegen I 2021a Hemispheric and seasonal contrast in cloud thermodynamic phase from a-train spaceborne instruments *J. Geophys. Res.: Atmos.* **126** e2020JD034322
- Vonnegut B and Chessin H 1971 Ice nucleation by coprecipitated silver iodide and silver bromide *Science* **174** 945–6
- Zängl G, Reinert D, Rípodas P and Baldauf M 2014 The icon (icosahedral non-hydrostatic) modelling framework of DWD and MPI-M: description of the non-hydrostatic dynamical core *Q. J. R. Meteorol. Soc.* **141** 563–79
- Zhang D, Wang Z, Kollias P, Vogelmann A M, Yang K and Luo T 2018 Ice particle production in mid-level stratiform mixed-phase clouds observed with collocated a-train measurements *Atmos. Chem. Phys.* **18** 4317–27
- Zhao M, Cao L, Duan L, Bala G and Caldeira K 2021 Climate more responsive to marine cloud brightening than ocean albedo modification: a model study *J. Geophys. Res.: Atmos.* **126** e2020JD033256